How to Cite: Andreeva, A.V., Baimuratova, R.K., Dorokhov, V.G., Akkuratov, A.V., Shilov, G.V., Kugabaeva, G.D., Golubeva, N.D., & Dzhardimalieva, G.I. (2024) Rational Synthesis of UiO-66 and its Application in the Hydrogenation Reaction of p-Chloronitrobenzene. *Eurasian Journal of Chemistry, 29, 3(115), 92–108.* https://doi.org/10.31489/2959-0663/3-24-10

Article

Received: 9 June 2024 | Revised: 29 July 2024 |
Accepted: 31 July 2024 | Published online: 19 August 2024

UDC 542.973+547.92

https://doi.org/10.31489/2959-0663/3-24-10

Anastasia V. Andreeva[1,2], Rose K. Baimuratova[1*], Victor G. Dorokhov[1], Alexander V. Akkuratov[1], Gennadii V. Shilov[1], Gulsara D. Kugabaeva[1,3], Nina D. Golubeva[1], Gulzhian I. Dzhardimalieva[1,3]

[1]Federal Research Center of Problems of Chemical Physics and Medicinal Chemistry, Russian Academy of Sciences, Chernogolovka, Russia;
[2]Lomonosov Moscow State University, Moscow, Russia;
[3]Moscow Aviation Institute (National Research University), Moscow, Russia
*(*Corresponding author's e-mail: Roz_Baz@mail.ru)*

Rational Synthesis of UiO-66 and its Application in the Hydrogenation Reaction of p-Chloronitrobenzene

Hydrogenation is a widely used reaction in the oil processing and industrial organic synthesis. UiO-66 is a promising porous organic-inorganic material that can be used as a support for catalytically active particles. The key part in the application of highly porous UiO-66 is the search of a simple synthesis method that meets international environmental standards. In this study, a "rational" method for the synthesis of MOFs was used to produce UiO-66. The use of pre-synthesized multinuclear zirconia clusters facilitates the synthesis of the desired network topology, enabling the process to be conducted in an environmentally friendly aqueous solution. The effects of reaction temperature, linker volume concentration and solvent type on the specific surface area and thermal properties were also evaluated in this work. We studied the composition, structure and physicochemical properties of the obtained compounds by IR spectroscopy, TGA and XRD analysis. The proposed procedure has been shown to yield UiO-66 with high specific surface area (S_{BET} = 885 m^2/g) and to extend the thermal stability range up to 490 °C. The post-synthetic modification of the obtained UiO-66 with the introduction of catalytically active Pd (Pd/UiO-66) was carried out, and high selectivity (83,0 %) of the obtained Pd/UiO-66 exhibited high selectivity in the hydrogenation reaction of p-chloronitrobenzene into p-chloroaniline in comparison with the traditional Pd/Al_2O_3.

Keywords: metal-organic frameworks, UiO-66, heterogeneous catalysts, Pd/UiO-66, hydrogenation, p-Chloronitrobenzene, zirconium complexes, terephthalic acid, hydrogenation of nitroderivatives.

1. Introduction

Metal-organic frameworks (MOFs) represent a novel class of porous materials that offer the potential for targeted structural design through the modification of either the coordinating metal or organic linkers. The extended surface area and porosity of MOFs render them suitable for a multitude of applications for gas storage [1] and separation [2], as photosensitive elements [3], electrolytes [4], adsorbents [5], drug delivery agents [6], sensor materials [7] and supports in catalytic systems [8]. Such variety of applications is related to the structure features (various shape and size of pores [9], surface area [10], high crystallinity, etc.) and limitless functional properties (magnetic [11], electrically conductive [12], etc.).

The use of MOFs [13] as supports for catalytically active agents [14] is one of the promising routes, because such structures have a homogeneous porous surface. Heterogeneous catalysis and the creation of novel types of heterogeneous catalysts [15] are actual directions for research; their development makes the important industrial processes easier and less expensive by avoiding the final product extraction from solutions [16]. Heterogeneous catalysts based on MOFs can be industrially utilized with concurrent execution of the following conditions: the obtained catalysts should demonstrate stable operation at low temperatures of hydrogenation process and be insensitive to various impurities contained in the feedstock, while retaining high catalytic activity or selectivity; maintain long lifetime and be suitable for regeneration with its production being inexpensive and compliant with enforceable environmental standards [17]. Therefore, this study employs a "rational" method for the synthesis of MOFs, entailing the use of polynuclear molecular complexes as a source of secondary building units (SBUs) [18–20]. Pre-synthesized multinuclear clusters directed the synthesis to the desired network topology; it makes it possible to eliminate toxic coordinating solvents

(DMF, DEF etc.) and to perform the synthesis in a green aqueous solution [21]. In addition, a rational approach to the preparation of MOFs avoids the drawbacks of standard solvothermal methods, leading to the formation of mixed phases and the production of polycrystalline or amorphous structures [22].

Zirconium (IV) [23] is the optimal candidate for use as a framework-forming metal in the creation of metal-organic coordination polymers (CPs) suitable for heterogeneous catalysis, due to the high chemical, mechanical and thermal stability of zirconium-based compounds. The hexanuclear Zr_6 nodes can be treated as a universal node for coordination of many organic linkers with various topologies. Such nodes have Lewis acid properties due to the presence of Zr^{4+} [24], and metal-organic frameworks based on them can directly act as catalysts [25]. Nevertheless, in this work the use of zirconium MOFs as a support for catalytically active particles is of interest.

In 2008, Cavka et al. [26] synthesized MOFs with $Zr_6(\mu^3\text{-}O)_4(\mu^3\text{-}OH)_4$ nodes and various ligands for the first time: terephthalic acid (UiO-66), 4,4'-biphenyl-dicarboxylic acid (UiO-67) and 4,4'-[p-terphenyl]-dicarboxylic acid (UiO-68). Due to the high coordination number of the zirconium cluster, these structures have a large specific surface area, high thermal, chemical and mechanical stability in comparison with other MOFs. However, UiO-66 is the most stable one, due to its smaller pore size. It is known that for porous materials there is a risk of collapse of the structure during solvent removal, and this effect intensifies with the increase of the pore size with longer linkers in UiO-67 and UiO-68 [27]. While embracing attractive and exceptional characteristics, these Zirconium-based metal-organic frameworks (Zr-MOFs) still require further exploration of their sensitivity towards synthesis conditions [28] and research for an optimal method for their preparation [29].

The outstanding physicochemical characteristics of UiO-66 became the basis for the application of these structures in fuel cells [30], catalysis [31, 22], and greenhouse gas adsorption [32]. Zr-MOFs are promising supports for catalytically active particles which are vastly utilized in hydrogenation reactions [33–35]. We have previously shown that catalytic systems based on Zr-MOFs of UiO-66 series with different linkers (1,4-benzene dicarboxylic, 2-amino-1,4-benzene dicarboxylic and 2,6-naphthalene dicarboxylic acids) demonstrate high selectivity in industrially significant reactions such as hydrogenation of phenylacetylene and allyl alcohol [36].

The reaction for generation of such important organic intermediates as halogenanilines which are widely used in industrial production of medicines, pesticides and pigments, remains highly relevant when catalytic properties of hydrogenation catalysts are studied [37]. The most common way to obtain such compounds is the reduction of the corresponding aromatic nitro derivatives by selective hydrogenation on transition metal catalysts [38]. However, high operating costs due to contamination of catalysts during the reaction and low selectivity hinder the widespread use of such approaches for the production of halogen-containing amines. In addition, the generation of hydrochloric acid due to dechlorination has an effect on the catalytic activity and often leads to reactor corrosion [39]. Deep hydrogenation and chlorine removal can be minimized by addition of inhibitors to the mixture; however this approach is based on a complicated mechanism with an increased number of variables that require careful consideration. Therefore, the development of a new type of catalysts that can selectively work under soft conditions represents a significant challenge.

Although, the concept of immobilization of nanoparticles onto MOFs matrices has recently been successfully demonstrated, attempt at synthesis of chemically stable MOFs based on $Zr_6(\mu^3\text{-}O)_4(\mu^3\text{-}OH)_4$ with high specific surface area in non-toxic solvents is a challenging task. Therefore, the aim of this research is to address the challenges associated with the development of catalytic hydrogenation systems based on a novel class of porous materials that can operate effectively under mild conditions, while also being cost-effective and in compliance with international environmental standards. The proposed approach involves a method for the synthesis of highly porous MOFs.

This work presents the optimization of the synthesis methodology of coordination polymer $[Zr_6O_4(OH)_4(C_8H_4O_4)_6]_n$ for the creation of UiO-66-based nanostructured Pd-containing heterogeneous catalyst with improved specific surface area and thermal properties. Furthermore the catalytic properties of the obtained Pd/UiO-66 in the hydrogenation reaction of p-chloronitrobenzene have been studied.

2. Experimental

2.1. Reactants and reagents

Potassium chloride (KCl, ch.pr.), palladium (II) chloride ($PdCl_2$, ch.pr.), zirconyl chloride octahydrate ($ZrOCl_2{\cdot}8H2O$, p.a.), terephthalic acid ($C_8H_6O_4$, TPA, p.a.), 1-chloro-4-nitrobenzene ($C_6H_4ClNO_2$, **ch.pr.**), acetic acid (CH_3COOH, p.a), sodium borohydride ($NaBH_4$, p.a), sodium hydroxide (NaOH, p.a.), anhydrous

γ-aluminum oxide powder (γ-Al_2O_3, SBET = 40–50 m^2/g, tech.), hydrochloric acid (HCl) were purchased from Ruskhim chemical company (Moscow, Russia) and were used without further purification). Polyethylene Glycol 1500 (PEG-1500, $H(OCH_2CH_2)_nOH$, for synthesis) was supplied by Aldrich company. Ethanol, acetonitrile, isopropyl alcohol and cyclohexene of REAKHIM grades were supplied by Chimmed Group and purified according to standard methods. The purity was confirmed by High-Performance Liquid Chromatography (HPLC).

2.2. Synthesis methods

2.2.1. Synthesis methodology of coordination polymer based on pre-synthesized cluster [$Zr_6O_4(OH)_4(CH_3COO)_{12}$]

1) In the initial stage of the procedure, 5 mL of 2M CH_3COOH was added dropwise to 5 mL of 1M $ZrOCl_2 \cdot 8H_2O$ to obtain a hexanuclear zirconium cluster according to the procedure from the literature [40]. The mixture was cured at 55 °C for 120 min.

2) At the next step, 0.814 g (4.9 mmol) of terephthalic acid dissolved in aqueous KOH or DMF solution according to Table 1 was added to the mixture to obtain UiO-66. For some experiments CH3COOH was also added to the TPA solution to increase the crystallinity of the obtained polymers. The mixture was left at the fixed temperature for 120 minutes upon the addition of the organic ligand solution. The obtained coordination polymers were extracted by centrifugation at 4500 rev/min and flushed with solvent several times. The samples were treated with methanol in a Soxhlet extractor (16 h, 70 °C) and subsequently dried in vacuum (10^{-3} Torr, 55 °C, 10 h) in order to remove the solvent that had been physically adsorbed in the pores.

Table 1

Conditions for the synthesis of samples representing MOFs of UiO-66 type

Sample	Solvent	Solvent volume, mL	Reaction temperature, °C	m(CH_3COOH), g	Mixing speed, rev/min
Sample 1	H_2O	25	25	–	200
Sample 2	H_2O	100	25	–	1000
Sample 3	H_2O	25	50	–	200
Sample 4	H_2O	25	75	–	200
Sample 5	DMF	15	25	–	200
Sample 6	H_2O	25	25	5.4	200
Sample 7	DMF	15	25	5.4	200

2.2.2. Methodology for encapsulation of Pd nanoparticles into the pores of metal-organic frameworks [36]

Using the selected sample, a heterogeneous catalyst was prepared at a rate of 0.5 % Pd per 1 g of support. To this end, 0.017 g (0.095 mmol) of $PdCl_2$ was dissolved in 100 mL of methanol in the presence of 0.019 g (0.254 mmol) of KCl to obtain the soluble salt K_2PdCl_4. Then 0.2 g of PEG-1500 and 1 g of coordination polymer were added to the solution. The mixture was kept for 150 minutes at 68 °C until the precipitate acquired a distinctive dark brown color. The product was extracted by centrifugation and subjected to vacuum drying (10^{-3} Torr, 55 °C, 10 h). The ratio of the reactants was increased up to 4 times to obtain a heterogeneous catalyst containing 2 % Pd.

2.2.3. Synthesis of a compare catalyst Pd/Al_2O_3

A solution of palladium chloride was added in portions of 2–3 mL to 100 mL of aqueous suspension of γ-Al_2O_3 with a concentration of 50 g/L heated to 50 °C. The reaction mixture was kept under stirring at magnetic stirrer (200 rev/min) and temperature 50 °C for one hour.

$PdCl_2$ (0.250 g, 1.41 mmol) was dissolved in 25 mL of water by adding 1.4 mL of 18.5 % HCl solution (7 mmol). Once the palladium chloride had been fully dissolved, the pH was increased to neutral (pH ≈ 6–7) by the addition of 1 M NaOH.

An alkaline aqueous solution of $NaBH_4$ (1.41 mmol, $m(NaBH_4)/m(NaOH)$ = 0,1) was added dropwise to the obtained suspension to recover Pd. The mixture was stepwise cured out at 50 °C for 30 minutes and at 90 °C for 30 minutes under stirring conditions on a magnetic stirrer (200 rev/min). The obtained catalyst was separated by filtration and dried in an oven (60 °C, 10 h).

2.3. Research techniques

2.3.1. X-ray diffraction

X-ray diffraction analysis of the samples was conducted on a powder diffractometer Aeris Benchtop (Malvern PANalytical, the Netherlands) in the range of scattering angles from 5 to 50 °C (scanning step 2θ — 0.002°C, emission — CuK_{α}, λ = 1,5406 Å).

2.3.2. Fourier transform infrared spectroscopy (FT-IR).

The identification of functional groups of the obtained compounds was carried out on a Perkin-Elmer Spectrum 100 infrared Fourier spectrometer (USA, 2006) equipped with an attachment for frustrated total internal reflection (FTIR) with a diamond prism for single reflection. The penetration depth for the material with deep refractive index (2.43) at 1000 cm^{-1} is 1.66 microns. FT-IR-FTIR spectra were recorded in the range of 360–4000 cm^{-1} at room temperature using 24 scans and the definition of 2 cm^{-1}. The baseline of the obtained spectra was corrected in the OPUS program.

2.3.3. Identification of specific surface area and porosity

The specific surface area of samples, average radius and pore size distribution were determined by low-temperature nitrogen adsorption (at 77 K) on the sorption analyzer "AUTOSORB-1" ("Quantachrome", USA) by static volumetric method. The interaction between adsorbent and adsorbate in porous solids occurs by physisorption process, which makes the specific surface area an important property. The Brunauer-Emmett-Teller (BET) model was used to determine the surface area of porous materials from the isotherms of N_2 gas adsorption. The BET method is based on the hypothesis of multilayer adsorption proceeding through the formation of a monolayer of adsorbent molecules on the adsorbate surface.

The shape of six types of adsorption-desorption isotherms gives information about the presence of micro- and mesopores, as well as the shape of pores if the isotherm has a hysteresis loop. The volume and surface of micropores were determined by the t-method, and the distribution of pore volume was plotted using the BJH theory [41].

2.3.4. Thermogravimetric analysis

The thermal stability of composites was evaluated by the temperature of the start of decarboxylation by thermogravimetric analysis using a TGA/SDTA851e METTLER TOLEDO thermal analyzer (Mettler Toledo, Switzerland). The samples were heated in a nitrogen atmosphere at a heating rate of 10 °C/min at a temperature range extending from 25 to 550 °C.

2.3.5. Elemental analysis

Elemental analysis was performed to determine the concentration of nanoparticles on the surface of catalytic systems. The Pd concentration was determined using the atomic absorption spectro-meter "AAS-3" (Zeiss, Germany).

2.3.6. Methodology for determination of catalytic activity

The process of hydrogenation of p-chloronitrobenzene (1.0 ± 0.001 g) was carried out in a duck-type non-flow glass reactor in isopropyl alcohol at fixed atmospheric hydrogen pressure (0.1 MPa) and temperature 48.5 °C under intensive stirring conditions (180–240 shakes per minute). The amounts of catalysts were 0.3 ± 0.005 g. Hydrogen was supplied to the reactor from a calibrated receiver with a water gate. The partial pressure of water vapor was subtracted from the total atmospheric pressure to determine the own gas pressure, then the gas volume was normalized. The catalyst was treated with hydrogen for 15 minutes in the reactor under stirring before the addition of p-chloronitrobenzene. The reaction rate was calculated graphically from the slope of the starting parts of the kinetic curves of hydrogen flow rate.

2.3.7. Methodology for the study of mixture composition

Progress of the hydrogenation of p-chloronitrobenzene was investigated by HPLC method on Helicon EX-1800 machine (Wufeng, China). Chromatograms were recorded on Orbit C18 column (150×4.6 mm, 5 mm) using acetonitrile/water mixture (6/4) at 40 °C and flow rate of 1 mL/min. The detector wavelengths were 254 and 290 nm.

3. Results and Discussion

3.1. Composition and structure of synthesized MOFs

The most common method for the obtaining of zirconium-based metal-organic coordination polymers is the direct mixing of the metal salt and the selected linker in DMF solution, as the majority of dicarboxylic aromatic acids are insoluble [42–46]. However, such process may lead to generation of different phases, which does not yield the desired structural topology [22, 47]. Accordingly, a "rational" method for the synthesis of MOFs, using polynuclear molecular complexes as sources of secondary building units, was em-

ployed in this work. Previously, we demonstrated the versatility of this approach to obtain a series of UiO-66 isostructural MOFs with different organic ligands (1,4-benzene dicarboxylic, 2-amino-1,4-benzene dicarboxylic, and 2,6-naphthalenedicarboxylic acids) [36]. However, the resulting MOFs exhibited reduced surface areas; therefore, the proposed methodology for the synthesis of UiO-66 coordination polymer was improved in this work.

A series of UiO-66-type MOFs was obtained through the initial formation of a hexanuclear zirconium acetate complex with further replacement of the acetic acid residues with terephthalic acid residues (Table 1).

The system of chemical equations describing the proposed low-temperature process of obtaining the UiO series coordination polymers with the terephthalic organic ligand is presented below:

Step 1. Formation of inorganic building block:

$$ZrCl_4 + H_2O \rightarrow ZrOCl_2 + 2HCl$$

$$6ZrOCl_2 + 12CH_3COOH \rightarrow Zr_6O_4(OH)_4(CH_3COO)_{12} + 12HCl \ pH \approx 1{,}5;\ 55\ °C$$

Step 2. Synthesis of UiO-66

$$C_8H_6O_4 + 2KOH \rightarrow K_2C_8H_4O_4 + 2H_2O$$

$$Zr_6O_4(OH)_4(CH_3COO)_{12} + 6K_2C_8H_4O_4 \rightarrow [Zr_6O_4(OH)_4(C_8H_4O_4)_6]_n + 12CH_3COOK$$

The impact of reaction temperature, linker volume concentration and solvent polarity on the specific surface area and thermal properties was also evaluated in this work (Table 1). It was shown that the increase of the reaction temperature up to 75 °C leads to the formation of mixed crystalline and amorphous products (Fig. 1, **Sample 4**). The use of DMF as a solvent resulted in the formation of a gel phase, which presented challenges in terms of solvent removal and the extraction of the pure product (Table 3).

3.1.1. Phase composition

The structures of the coordination polymers were confirmed by X-ray diffraction analysis. Most of the obtained samples had X-ray diffractograms with narrow diffraction maximums, it indicates the mainly crystalline-lytic phase state (Fig. 1). The observed peaks position agrees with the calculated spectrum taken from the literature [26] and confirms the structure of the samples. The formation of mixed phases with increasing synthesis temperature is confirmed by detecting multiple secondary reflections on the X-ray diffraction pattern of **Sample 4** (reaction temperature — 75 °C). Additionally the formation of by-products is observed with increasing temperature (2 Θ° ≈ 28,43). The formation of an arm below 7° for **Sample 5** obtained in DMF may be associated with the reflection plane 110 and reo phase defects [48–50]. The broadening of the main peak, can also be attributed to the presence of defects in the structure, which may be explained by the competition between acetic and terephthalic acids for carboxylate sites on $Zr_6O_4(OH)_4(COO)_{12}$ clusters [49]. It is known that defects in the structure of MOFs increase the catalytic activity indicating that inorganic nodes can be conceptualized as Lewis/Brønsted centers [51, 52].

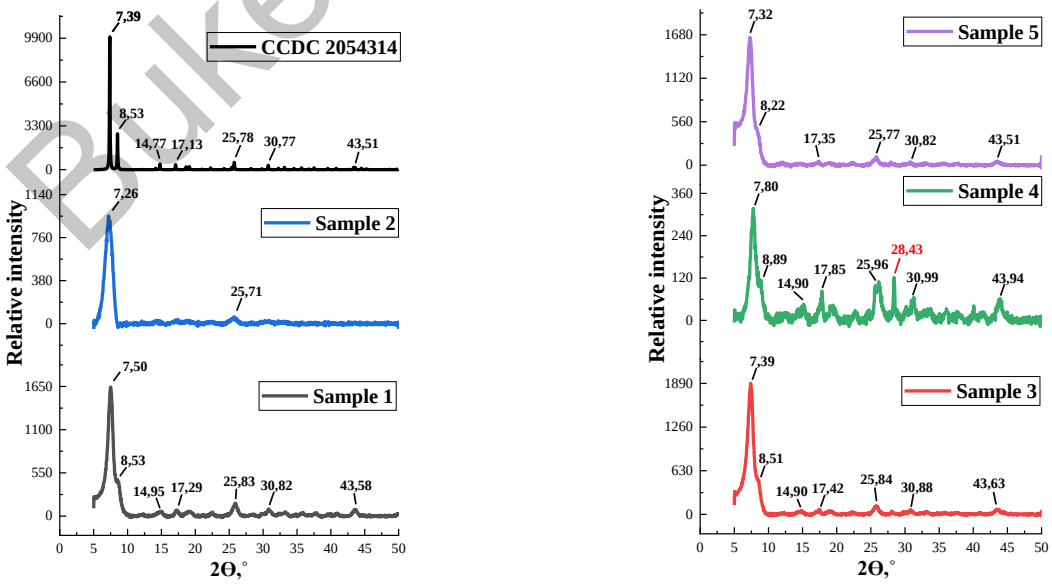

Figure 1. X-ray diffraction patterns of synthesized MOFs

3.1.2. Identification of functional groups by FTIR-ATR spectroscopy

The primary obtaining of the hexanuclear zirconium acetate complex $Zr_6O_4(OH)_4(COO)_{12}$ with the formation of coordination polymers by replacement of the acetic acid residues with terephthalic acid residues occurs during the synthesis. However, the exchange reaction may not occur completely in the case of high temperature synthesis, as evidenced by the detection of absorption bands characteristic of terephthalic acid (Fig. 2). For instance, bands of asymmetric vibrations of the –CO (in COO^-) appear in the region of 1676 $см^{-1}$ for **Samples 3** and **4**. Probably, the formation of the target product occurs worse at high temperatures of UiO-66 coordination polymer synthesis. This may be due to unfavorable reactions, which suggests that a temperature range limitation is necessary for the target exchange reaction. For **Sample 5**, the intensity of the –CO bond bands was lower, but the presence of the non-reacted acid band was also observed. The specific for the Zr–O bond absorption bands at 470 cm^{-1} were observed for each of the samples.

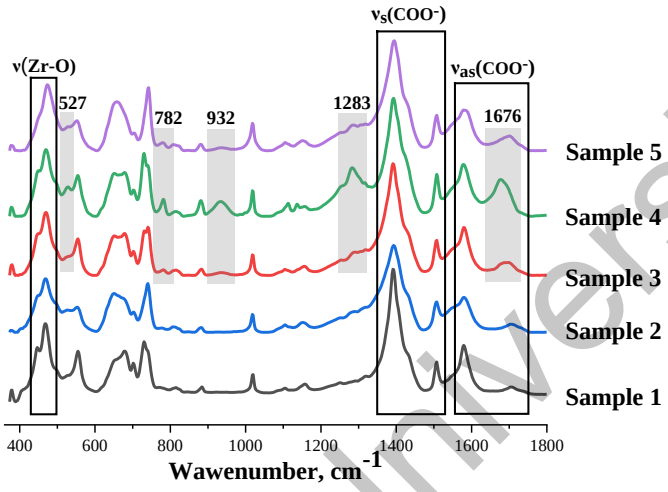

Figure 2. FTIR-ATR spectra of synthesized MOFs

The addition of modulator can reduce the rate of nucleation and delay crystal growth. Consequently, it leads to the formation of highly crystalline coordination polymers (examples of this approach are known from the literature [53]). Therefore, we attempted to improve the crystallinity of the samples by adding excess of acetic acid. The samples were obtained in aqueous solution (**Sample 6**) and in DMF (**Sample 7**) and their structures were studied by IR spectroscopy (Figure 3). IR spectra of the obtained samples are totally identical to the spectrum of the initial ligand. That demonstrated the impossibility of formation of the coordination polymer structure under these conditions. Therefore, we demonstrated the impracticality of increasing the amount of acetic acid to achieve higher crystallinity in the case of the used methodology.

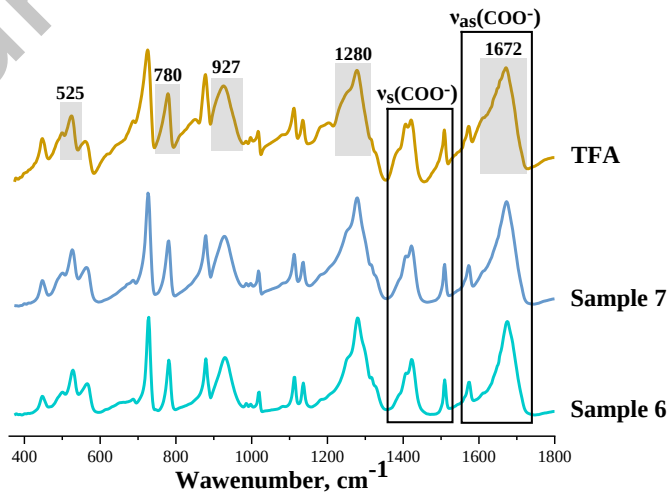

Figure 3. FTIR-ATR spectra of samples synthesized with addition of excessive acetic acid during the synthesis compared to the original ligand (TPA)

3.1.3 Results of the study of specific surface area

The major property of supports of catalytically active particles is the developed specific surface area; therefore, it was important to evaluate this property of the obtained coordination polymers. According to the nitrogen adsorption-desorption isotherms (Fig. 4), all the obtained MOFs have developed specific surface area. The isotherms are classified as type IV according to the IUPAC classification, with a hysteresis loop indicating the mesoporous structure of the samples. The hysteresis shape of the isotherm of **Sample 1** indicates nearly cylindrical pores (type H1). The other samples have an irregular, more chaotic pore structure with hysteresis type H2.

In order to characterize the porosity of the obtained catalysts in details, the external surface area was estimated. It is known that nanoparticles of catalytically active metal can potentially be localized directly in external pores ($S_{external}$ / S_{BET}). It is shown that the use of terephthalic acid solution at low volume concentration during synthesis (**Sample 2**) leads to a considerable proportion of the external surface area of the obtained coordination polymer accounting for approximately 60 %. **Sample 2** has the highest share of external surface area, so it was selected for further use as a support for catalytically active particles (Table 2).

The share of micropores unsuitable for encapsulation of Pd nanoparticles grows with increasing reaction temperature (**Samples 3**, **4**); therefore, it was optimal to carry out the synthesis at room-temperature. It should be noted that the determined values of specific surface area for UiO-66 are comparable to the values obtained in DMF, but they remain below the theoretical maximum (Table 4).

Table 2

Specific surface area, volume of pores and average pore diameter of the synthesized MOFs

Sample	S_{BET}, m^2/g	V_p, cm^3/g	Average pore diameter, nm	t-method		
				S_{micro}, m^2/g	$S_{external}$, m^2/g	$S_{external}$/ S_{BET}, %
Sample 1	885 ± 71	0.80 ± 0.06	8.9 ± 0.7	362 ± 72	523 ± 42	59.1
Sample 2	707 ± 57	0.29 ± 0.02	3.6 ± 0.3	193 ± 39	514 ± 41	72.7
Sample 3	726 ± 58	0.23 ± 0.02	3.6 ± 0.3	389 ± 78	338 ± 27	46.5
Sample 4	760 ± 61	0.28 ± 0.02	3.6 ± 0.3	402 ± 80	359 ± 29	47.1
Sample 5	801 ± 64	0.53 ± 0.04	6.0 ± 0.5	383 ± 78	418 ± 33	52.2

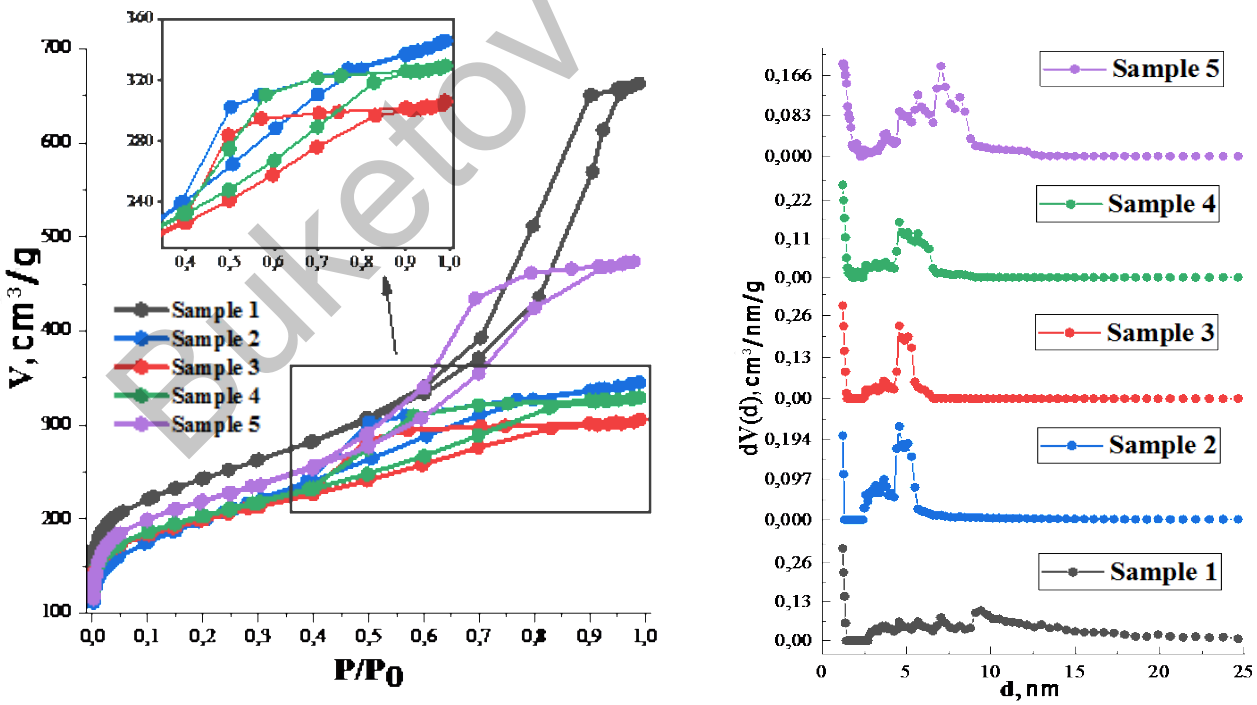

a *b*

Figure 4. Nitrogen adsorption-desorption isotherms (a) and pore size distribution (b) of the synthesized MOFs

3.1.4. The results of the thermal stability

All samples have three stages of mass loss according to the TGA curves (Fig. 5). The first stage, at temperatures up to 200 °C, involved the elimination of the residual solvent physically adsorbed in the pores of the coordination polymers. This high temperature of mass loss is caused by strong coordinating interactions. The following step included decarboxylation. A deeper decomposition of the coordination polymer framework with the formation of zirconium oxide occurred at temperatures above 450 °C.

Sample 5, synthesized using DMF solvent, contained more sorbed solvent molecules and had the lowest temperature of 10 % mass loss at the first stage of decomposition (207 °C) (Table 3). This may be caused by the formation of a gel phase during synthesis, making it difficult to remove the solvent when drying the sample, as well as the stronger interactions between DMF molecules and zirconium metal centers [54].

Table 3

Results of thermogravimetric analysis of UiO-66 samples obtained under different conditions

Sample	$T_{5\,\%}$, °C	$T_{10\,\%}$, °C	$T_{20\,\%}$, °C	$T_{30\,\%}$, °C	T_{max}, °C	$\Delta m_{25\text{-}450}$, mass %	Residual mass at 600 °C, mass %
Sample 1	345	490	539	554	552	7,6	43,7
Sample 2	161	333	527	553	557	12,9	46,7
Sample 3	165	337	532	557	554	12,6	41,6
Sample 4	180	341	529	555	557	13,1	42,9
Sample 5	111	206	512	546	553	15,6	47,3

Note – *$T_{5\,\%}$, $T_{10\,\%}$, $T_{20\,\%}$, $T_{30\,\%}$ — temperatures of 5 %, 10 %, 20 %, 30 % mass loss; T_{max} — temperature of maximum decomposition rate according to DTG curve*

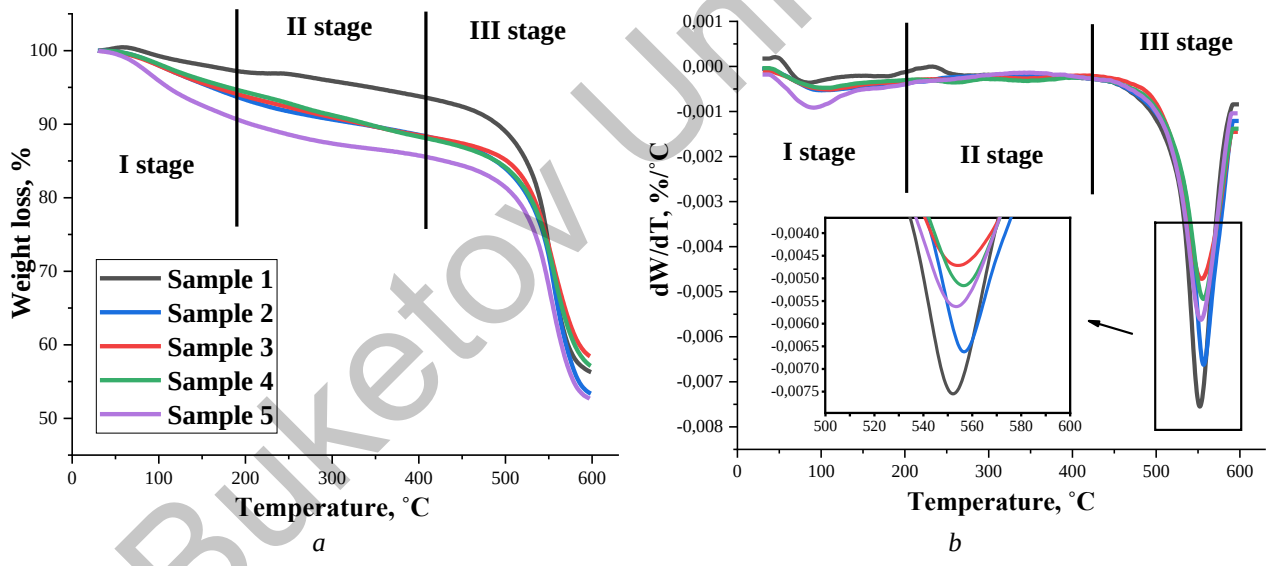

Figure 5. TGA curves (*a*) and their differential form (*b*) of UiO-66 samples obtained under different conditions

The results of thermogravimetric analysis demonstrated high thermal stability of the samples and the potential for practical application at temperatures up to 450 °C. Moreover, for **Sample 1**, the mass loss at this temperature was about 7.6 %, indicating the absence of decarboxylation with preservation of structure at high temperatures.

As a result of this research, a sample indicated as **Sample 1** was selected as a support, having an optimal surface area with a high share of external pores (which can potentially be filled with catalytically active metal nanoparticles), high thermal stability and chemical purity.

The physicochemical properties of the investigated coordination polymer were compared with the previously obtained sample [36] ($[Zr_6O_4(OH)_4(terephthalic\ acid)_{12}]_n$, S_{BET} = 360 ± 29 m^2/g, $T_{10\,\%}$ = 146.62 ± 0.01 °C). As a result, the present method provides a 2,5-fold increase of the specific surface area from 360 to 885 m^2/g and extends the range of thermal stability up to 490 °C (Table 4). Solvothermal, microwave, electrochemical or mechanical methods are most commonly used to produce UiO-66. It is noted that the use of

microwave oven can increase the nucleation rate of synthesis and electrochemical methods can provide more accurate control of process parameters [43, 45, 55, 56]. Most of the methods use DMF as solvent, and modulation approaches restricting crystal growth are used to obtain more crystalline products. The major significance for the formation of the target structure in such reactions is the molar ratio of modulator and Zr [50]. In this work, the increase of modulator amount above equimolar values prevented the formation of the desired structure in aqueous solution synthesis. Obviously, the concentration of the modulator plays a crucial role in the formation of UiO-66, as it is necessary to select the concentration of the competing ligand to achieve a process that limits crystal growth.

Table 4

Comparison table of physicochemical properties of UiO-66 obtained under different reaction conditions

Sample	Synthesis conditions	$T_{10\,\%}$, °C	S_{BET}, m^2/g	Ref.
$[Zr_6O_4(OH)_4(TFA)_{12}]_n$(UiO-66)	$ZrCl_4$, CH_3COOH, H_2O, 55 °C	146,62 ± 0,01	360 ± 29	[36]
$[Zr_6O_4(OH)_4(TFA)_{12}]_n$(UiO-66)	$ZrOCl_2$, CH_3COOH, H_2O, 25 °C	490,54 ± 0,01	885 ± 71	This work
UiO-66	$ZrCl_4$, DMF, 120 °C	-	410	[50]
UiO-66	$ZrCl_4$, HCl, DMF, 120 °C	-	212-1647	[50]
UiO-66	$ZrCl_4$, DMF/H_2O = 100, 120°C.	-	940	[54]
UiO-66	$Zr(OnPr)_4$, DMF/1-propanol, CH_3COOH, 25°	-	960-1290	[57]
UiO-66	$ZrOCl_2$, DMF, 60 °C	-	634	[58]

3.2. Catalytic properties of the synthesized Pd-doped catalysts

3.2.1. Hydrogenation of cyclohexene

Catalytic system was synthesized based on the obtained coordination polymer by applying of 0,5 wt% palladium nanoparticles on 1 gram of support and three cycles of cyclohexene hydrogenation reaction were carried out to compare and evaluate the catalytic activity.

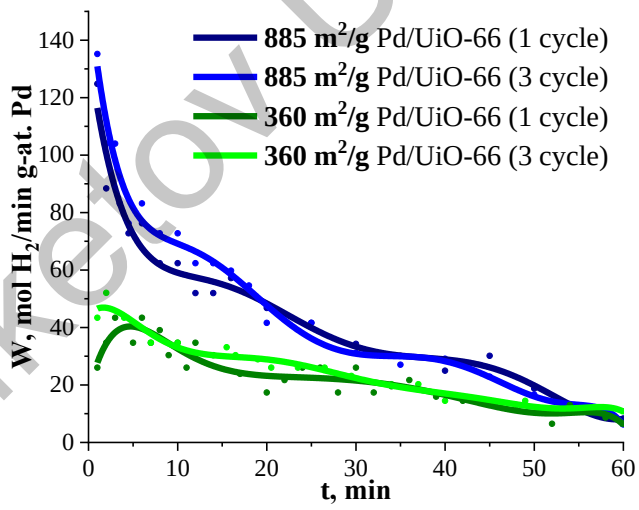

Figure 6. Dependence of cyclohexene hydrogenation rate on the reaction time in repeated cycles

Figure 6 shows that the use of the obtained coordination polymer with improved characteristics increased the initial hydrogenation rate by 3 times and reduced the total process time from ~90 to ~60 minutes.

3.2.2. Hydrogenation reaction of p-chloronitrobenzene

The catalytic properties were investigated in the industrially important hydrogenation reaction of p-chloronitrobenzene. Selective hydrogenation of nitro derivatives of benzene to obtain halogen substituted products is an important problem, since such compounds are widely used in the production of drugs, pesticides and pigments [37]. In addition, the dechlorination of benzene amino derivatives is often accompanied by the release of active chlorine and hydrochloric acid (Scheme 1), leading to corrosion and environmental pollution [39], so minimizing of this process is an important issue.

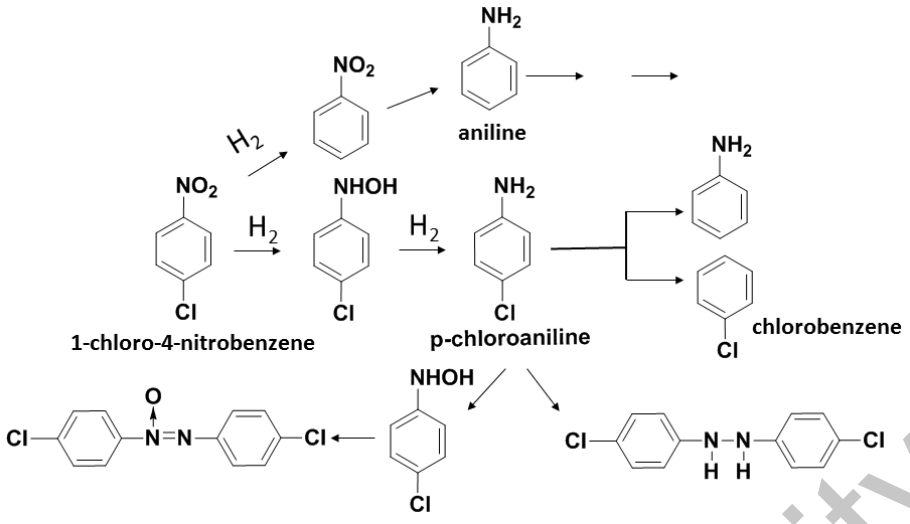

Scheme 1. Main paths of nitrochlorobenzene hydrogenation reaction

The catalytic system comprising Pd 1.7 ± 0.1 wt.%/g of support was obtained based on the synthesized **Sample 1**. Its characteristics were compared with the commercial Pd/Al_2O_3 catalyst (palladium content — 1.8 ± 0.1 wt.%).

The X-ray diffractogram profile of the Pd/UiO-66 catalyst is identical to the X-ray diffractogram of the initial MOFs, it indicates the preservation of the structure after the Pd nanoparticles deposition. Reflexes at 2 Θ° ≈ 40.12; 46.66; 68.12 corresponding to the metal Pd can be found on the X-ray diffractogram (Pd (46-1043), Fig. 7). The identification of Pd on Al_2O_3 is difficult due to the overlap of the support peaks.

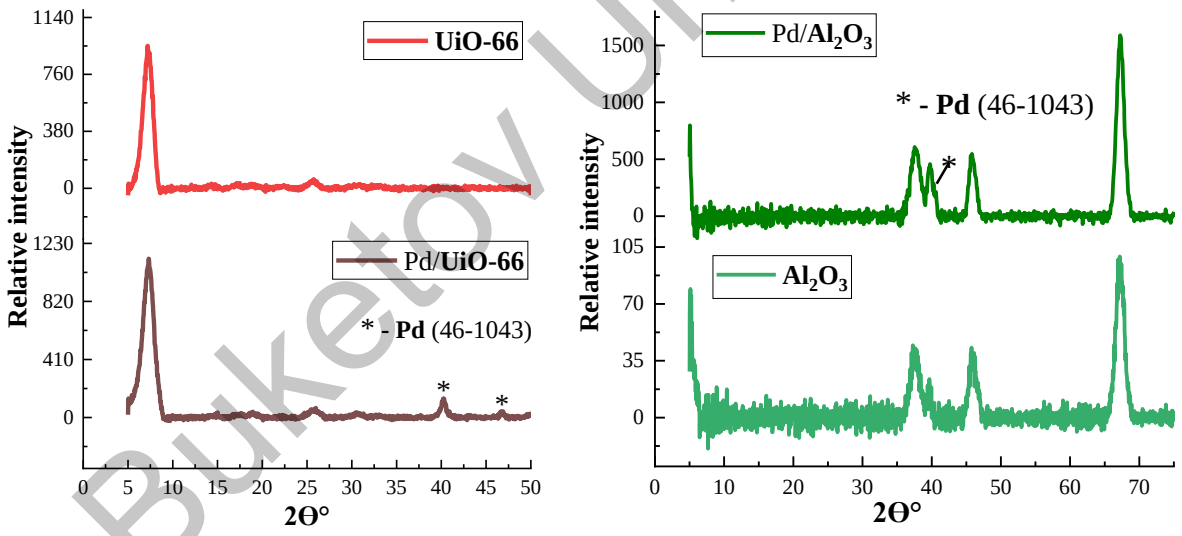

Figure 7. X-ray diffraction patterns of the obtained catalysts before and after palladium deposition

The morphology and distribution of palladium were analyzed by TEM microscopy. The homogeneous distribution of palladium nanoparticles on the surface of the coordination polymer UiO-66 can be seen in the presented TEM photographs (Fig. 8). Other situation is observed for the industrial support of catalytically active particles (Al_2O_3). The nanoparticles are aggregated on the surface of aluminum oxide. Particles with sharp edges of the inhomogeneous shape of the initial Al_2O_3 can be seen in TEM images with a resolution of 0.5 μ. The average size of particles on the surface of the analyzed catalytic systems ranged from 5 to 20 nm (Fig. 9).

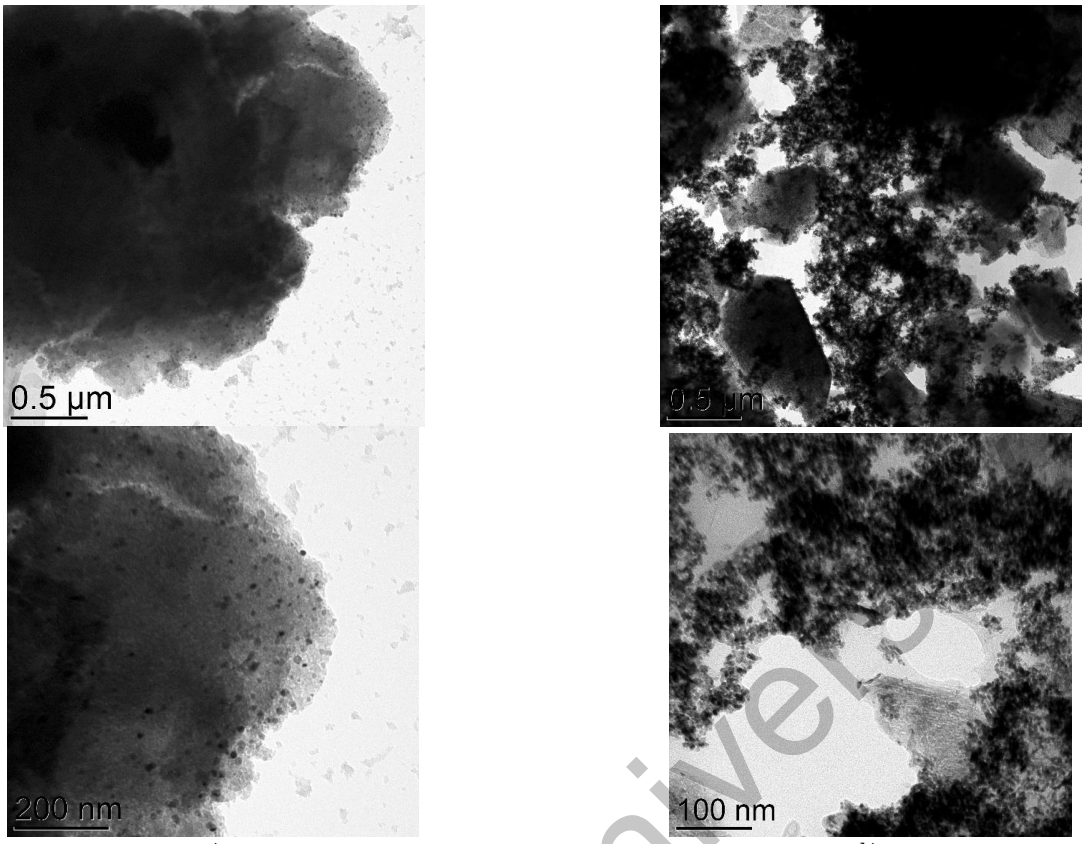

a) *b*)

Figure 8. TEM images of the Pd/UiO-66 (a) and Pd/Al_2O_3 (b) surface

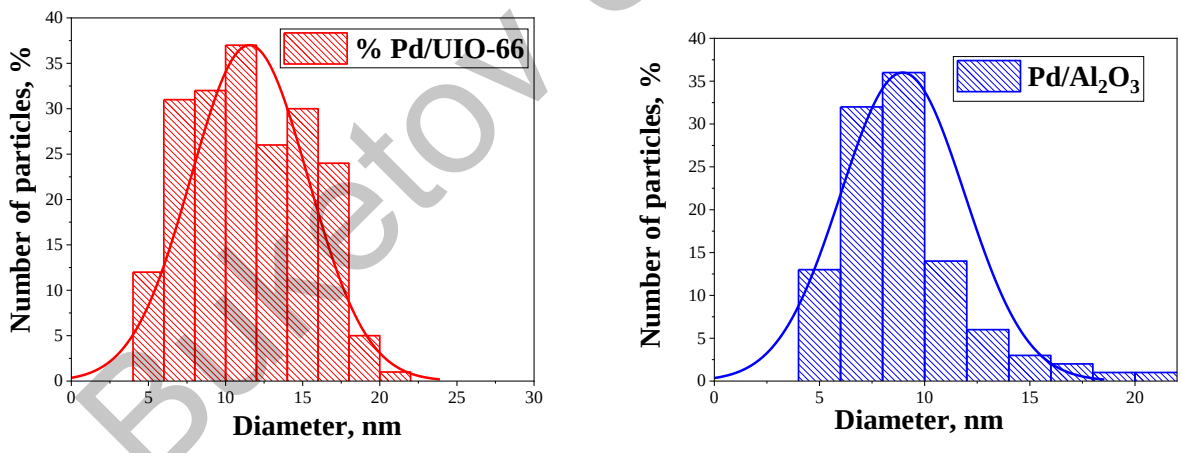

Figure 9. Histograms of Pd nanoparticle size distribution derived from TEM images

High-Performance Liquid Chromatography (HPLC) was used to analyze the time-dependent change of the mixture composition during the hydrogenation reaction. During the hydrogenation of p-chloronitrobenzene in the presence of Pd/Al_2O_3, the aniline content in the mixture was about ~20 % four minutes after the start of the process (Fig. 10). The complete conversion of the substrate was achieved after ten minutes, but the hydrogenation rates remained sufficiently high to ultimately result in a dechlorination process and the formation of unidentified reaction by-products.

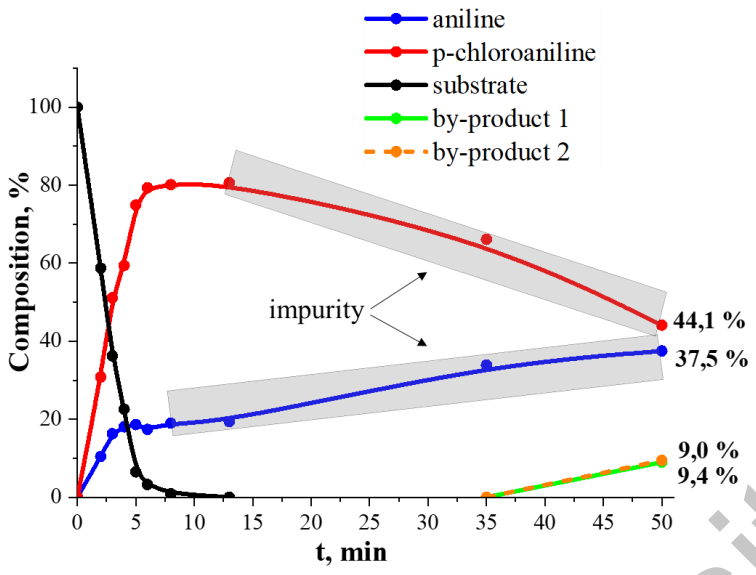

Figure 10. Dependence of reaction mixture composition on time during hydrogenation of p-chloronitrobenzene on the Pd/Al_2O_3 catalyst

The hydrogenation of p-chloronitrobenzene on the proposed Pd/UiO-66 catalytic system proceeded significantly longer. It may be explained by successive processes of adsorption and desorption of substrate in MOF pores before interaction with Pd active centers. Nevertheless, the observed reaction occurred with high selectivity of ~83 % up to the formation of p-chloroaniline (Fig. 11).

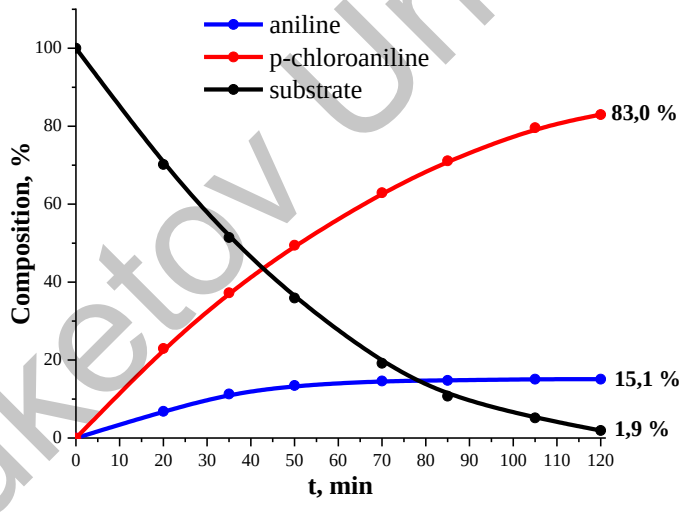

Figure 11. Dependence of reaction mixture composition on time during hydrogenation of p-chloronitrobenzene on the Pd/UiO-66 catalyst

Figure 12 shows the chromatograms of hydrogenation reaction products obtained by the process on two catalysts. In the case of Pd/Al_2O_3, the formation of many unidentified by-products (red circles on the chromatogram) leads to impurity of the target product (p-chloroaniline) and a decrease of selectivity below 44 %.

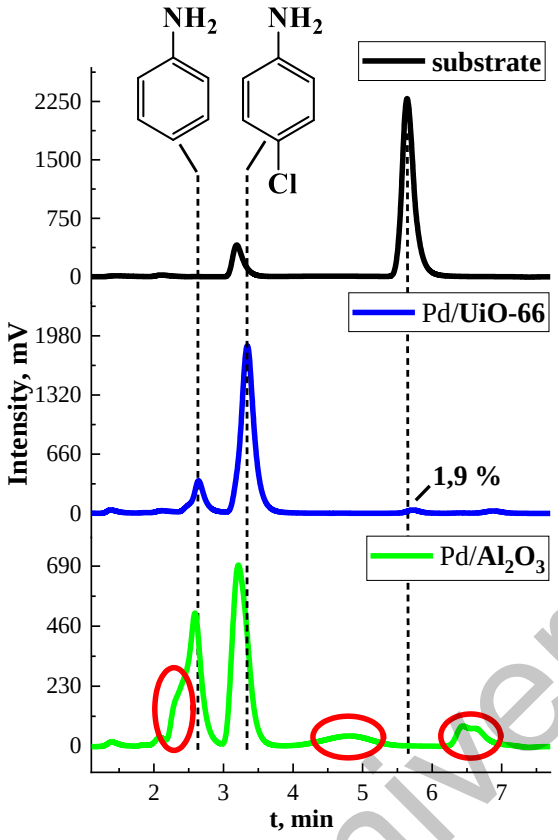

Figure 12. HPLC of the hydrogenation reaction mixture on different catalysts at a hydrogen consumption rate w(H_2) < 0.6 mL/min

In turn, using of the suggested catalytic system Pd/UiO-66 enables to obtain pure p-chloroaniline with high selectivity (83.0 %) at 98.1 % conversion (Table 5).

Table 5

Results of hydrogenation reaction of p-chloronitrobenzene using synthesized catalysts

Catalysts	P-chloraniline selectivity, %	Conversion, %
Pd/UiO-66	83,0	98,1
Pd/Al_2O_3	<44	100

Note – The conditions of the experiment: m_{cat} = 0,300 g; m_{sub} = 1,000 g; solvent — isopropanol (40 mL); T = 48,5 °C; p = 1 atm.

4. Conclusions

In this study, UiO-66 was obtained using a “rational” method for the synthesis of MOFs in aqueous solution. We demonstrated that increasing synthesis temperature from 25 °C to 75 °C lead to the increase of the share of micropores in the structure, as well as to the formation of amorphous MOFs and other by-products. The use of DMF as a solvent in this approach led to the formation of gel phase, complicating the removal of solvent and extraction of pure product. The addition of a modulator (acetic acid) in excess of equimolar quantities prevented the formation of the desired structure.

The composition, structure and physicochemical properties of the obtained compounds were studied by IR spectroscopy, TGA and XRD analysis. The results demonstrate that the proposed methodology effectively enhances the specific surface area by 2.5 times from 360 to 885 m^2/g and extends the range of thermal stability up to 490 °C.

The catalytic system Pd/UiO-66 was prepared through the post-synthetic modification of the obtained UiO-66 by encapsulation of catalytically active Pd. The ability of the obtained catalyst to carry out the reaction with high selectivity (83.0 %), in comparison with traditional Pd/Al_2O_3, was shown in the hydrogenation reaction of p-chloronitrobenzene to p-chloroaniline.

The use of pre-synthesized inorganic building blocks $Zr_6(\mu^3\text{-}O)_4(\mu^3\text{-}OH)_4$ demonstrates the potential of a rational stepwise approach for the synthesis of UiO-66, and could be a low-temperature scalable eco-friendly way to produce such highly porous materials.

Funding

This work has been carried out in accordance with the state tasks, state registration 124013000757-0, 12211170004-8, and 124013000722-8 using the equipment of the Multi-User Analytical Center of FRC PCP and MC RAS.

*Author Information**

**The authors' names are presented in the following order: First Name, Middle Name and Last Name*

Anastasia Vyacheslavovna Andreeva — Graduate Student, Department of Fundamental Physical and Chemical Engineering, Lomonosov Moscow State University, 119991, Moscow, Russia; Laboratory Assistant, Federal Research Center of Problems of Chemical Physics and Medicinal Chemistry, Russian Academy of Sciences, 142432, Chernogolovka, Moscow region, Russia; e-mail: andreevaav13@yandex.ru

Rose Kurmangalievna Baimuratova *(corresponding author)* — Candidate of Chemical Sciences, Junior Researcher, Federal Research Center of Problems of Chemical Physics and Medicinal Chemistry, Russian Academy of Sciences, 142432, Chernogolovka, Moscow region, Russia; e-mail: roz_baz@mail.ru; https://orcid.org/0000-0002-8389-6871

Victor Grigorievich Dorokhov — Candidate of Chemical Sciences, Head of Laboratory of Catalytic Synthesis of Organic Compounds, Federal Research Center of Problems of Chemical Physics and Medicinal Chemistry, Russian Academy of Sciences, 142432, Chernogolovka, Moscow region, Russia; e-mail: vicd@icp.ac.ru

Alexander Vitalievich Akkuratov — Candidate of Chemical Sciences, Head of Laboratory of Photosensitive and Electroactive Materials Department of Polymers and Composite Materials, Federal Research Center of Problems of Chemical Physics and Medicinal Chemistry, Russian Academy of Sciences, 142432, Chernogolovka, Moscow region, Russia; e-mail: akkuratow@yandex.ru; https://orcid.org/0000-0001-8750-0048

Gennadii Viktorovich Shilov — Candidate of Physical and Mathematical Sciences, Senior Researcher, Federal Research Center of Problems of Chemical Physics and Medicinal Chemistry, Russian Academy of Sciences, 142432, Chernogolovka, Moscow region, Russia; e-mail: genshil@icp.ac.ru

Gulsara Damirovna Kugabaeva — PhD Student, Moscow Aviation Institute (National Research University), 125993, Moscow, Russia; Junior Researcher, Federal Research Center of Problems of Chemical Physics and Medicinal Chemistry, Russian Academy of Sciences, 142432, Chernogolovka, Moscow region, Russia; e-mail: gulsara_kugabaev@mail.ru

Nina Danilovna Golubeva — Senior Researcher, Federal Research Center of Problems of Chemical Physics and Medicinal Chemistry, Russian Academy of Sciences, 142432, Chernogolovka, Moscow region, Russia; e-mail: nd_golubeva@mail.ru

Gulzhian Iskakovna Dzhardimalieva — Doctor of Chemical Sciences, Head of Laboratory of Metallopolymers, Federal Research Center of Problems of Chemical Physics and Medicinal Chemistry, Russian Academy of Sciences, 142432, Chernogolovka, Moscow region, Russia; e-mail: dzhardim@icp.ac.ru; https://orcid.org/0000-0002-4727-8910

Author Contributions

The manuscript was written through contributions of all authors. All authors have given approval to the final version of the manuscript. CRediT: **Anastasia Vyacheslavovna Andreeva** investigation, visualization, writing-original draft; **Rose Kurmangalievna Baimuratova** conceptualization, methodology, data curation, writing-review & editing; **Victor Grigorievich Dorokhov** investigation, methodology, data curation, supervision; **Alexander Vitalievich Akkuratov** investigation, methodology, data curation; **Shilov Gennadii Viktorovich** investigation, formal analysis; **Gulsara Damirovna Kugabaeva** validation, data curation, for-

mal analysis; **Golubeva Nina Danilovna** data curation, formal analysis, validation; **Gulzhian Iskakovna Dzhardimalieva** conceptualization, data curation, resources, supervision, writing-review & editing.

Conflicts of Interest

The authors declare no conflict of interest.

References

1 Li, B., Wen, H.-M., Zhou, W., & Chen, B. (2014). Porous Metal–Organic Frameworks for Gas Storage and Separation: What, How, and Why? *The Journal of Physical Chemistry Letters, 5*(20), 3468–3479. https://doi.org/10.1021/jz501586e

2 Semerci, F., Yeşilel, O. Z., Soylu, M. S., Keskin, S., & Büyükgüngör, O. (2013). A two-dimensional photoluminescent cadmium(II) coordination polymer containing a new coordination mode of pyridine-2,3-dicarboxylate: Synthesis, structure and molecular simulations for gas storage and separation applications. *Polyhedron, 50*(1), 314–320. https://doi.org/10.1016/j.poly.2012.10.009

3 Wang, H., Liu, Z., Liu, Z., Jiang, J., & Li, G. (2021). Photo-Dissociable Fe $^{3+}$ -Carboxylate Coordination: A General Approach toward Hydrogels with Shape Programming and Active Morphing Functionalities. *ACS Applied Materials & Interfaces, 13*(49), 59310–59319. https://doi.org/10.1021/acsami.1c19458

4 Liu, J., Zheng, M., Wu, S., & Zhang, L. (2023). Design strategies for coordination polymers as electrodes and electrolytes in rechargeable lithium batteries. *Coordination Chemistry Reviews, 483*, 215084. https://doi.org/10.1016/j.ccr.2023.215084

5 Xiao, L., Xiong, Y., Tian, S., He, C., Su, Q., & Wen, Z. (2015). One-dimensional coordination supramolecular polymer [Cu(bipy)(SO4)]n as an adsorbent for adsorption and kinetic separation of anionic dyes. *Chemical Engineering Journal, 265*, 157–163. https://doi.org/10.1016/j.cej.2014.11.134

6 Xiang, S., Liu, J., Han, G., Zhang, W., Long, Y., Deng, Y., Wang, B., & Weng, Q. (2023). Design of red-emitting 1D zinc coordination polymer for targeted drug delivery to nucleus. *Chemical Engineering Journal, 470*, 144177. https://doi.org/10.1016/j.cej.2023.144177

7 Shukla, A. K., Verma, V., Goriyan, P., Rani, A., Verma, A., Singh, A., Yadav, B. C., Baimuratova, R. K., Andreeva, A. V., & Dzhardimalieva, G. I. (2024). Zr6O4(OH)4 Based Metal-Organic Frameworks for the Enhanced Chemiresistive Sensing of Ethanol. *Journal of Inorganic and Organometallic Polymers and Materials*, 1–16. https://doi.org/10.1007/s10904-023-02986-1

8 Bavykina, A., Kolobov, N., Khan, I. S., Bau, J. A., Ramirez, A., & Gascon, J. (2020). Metal–Organic Frameworks in Heterogeneous Catalysis: Recent Progress, New Trends, and Future Perspectives. *Chemical Reviews, 120*(16), 8468–8535. https://doi.org/10.1021/acs.chemrev.9b00685

9 De Almeida, F. B., Da Silva Cunha, M., Barros, W. P., De Abreu, H. A., & Diniz, R. (2020). Structure, Electronic, Magnetic, and Gas Adsorption Properties of Zinc(II) and Cobalt(II) Coordination Polymers Assembled from Isonicotinylhydrazine and Trimesic Acid. *The Journal of Physical Chemistry C, 124*(38), 21103–21112. https://doi.org/10.1021/acs.jpcc.0c06479

10 Wang, J., Fan, Y., Tan, Y., Zhao, X., Zhang, Y., Cheng, C., & Yang, M. (2018). Porphyrinic Metal–Organic Framework PCN-224 Nanoparticles for Near-Infrared-Induced Attenuation of Aggregation and Neurotoxicity of Alzheimer's Amyloid-β Peptide. *ACS Applied Materials & Interfaces, 10*(43), 36615–36621. https://doi.org/10.1021/acsami.8b15452

11 Agarwal, R. A., Aijaz, A., Sañudo, C., Xu, Q., & Bharadwaj, P. K. (2013). Gas Adsorption and Magnetic Properties in Isostructural Ni(II), Mn(II), and Co(II) Coordination Polymers. *Crystal Growth & Design, 13*(3), 1238–1245. https://doi.org/10.1021/cg3016904

12 Zhang, C., Fan, K., Chen, Y., Wu, Y., & Wang, C. (2021). Conjugated Coordination Polymers as Electrodes for Rechargeable Batteries. *ACS Applied Electronic Materials, 3*(5), 1947–1958. https://doi.org/10.1021/acsaelm.1c00297

13 Sánchez-Serratos, M., Raziel Álvarez, J., González-Zamora, E., & Ibarra, I. A. (2017). Porous Coordination Polymers (PCPs): New Platforms for Gas Storage. *Journal of the Mexican Chemical Society, 60*(2). https://doi.org/10.29356/jmcs.v60i2.72

14 Wang, Q., & Astruc, D. (2020). State of the Art and Prospects in Metal–Organic Framework (MOF)-Based and MOF-Derived Nanocatalysis. *Chemical Reviews, 120*(2), 1438–1511. https://doi.org/10.1021/acs.chemrev.9b00223

15 Huang, Y. -B., Wang, Q., Liang, J., Wang, X., & Cao, R. (2016). Soluble Metal-Nanoparticle-Decorated Porous Coordination Polymers for the Homogenization of Heterogeneous Catalysis. *Journal of the American Chemical Society, 138*(32), 10104–10107. https://doi.org/10.1021/jacs.6b06185

16 Dhakshinamoorthy, A., Asiri, A. M., & Garcia, H. (2019). Formation of C–C and C–Heteroatom Bonds by C–H Activation by Metal Organic Frameworks as Catalysts or Supports. *ACS Catalysis, 9*(2), 1081–1102. https://doi.org/10.1021/acscatal.8b04506

17 Guo, M., Zhang, M., Liu, R., Zhang, X., & Li, G. (2022). State-of-the-Art Advancements in Photocatalytic Hydrogenation: Reaction Mechanism and Recent Progress in Metal-Organic Framework (MOF)-Based Catalysts. *Advanced Science, 9*(1), 2103361. https://doi.org/10.1002/advs.202103361

18 Ockwig, N. W., Delgado-Friedrichs, O., O'Keeffe, M., & Yaghi, O. M. (2005). Reticular Chemistry: Occurrence and Taxonomy of Nets and Grammar for the Design of Frameworks. *Accounts of Chemical Research, 38*(3), 176–182. https://doi.org/10.1021/ar020022l

19 Yaghi, O. M., O'Keeffe, M., Ockwig, N. W., Chae, H. K., Eddaoudi, M., & Kim, J. (2003). Reticular synthesis and the design of new materials. *Nature, 423*(6941), 705–714. https://doi.org/10.1038/nature01650

20 Baimuratova, R. K., Zhinzhilo, V. A., Uflyand, I. E., Dmitriev, A. I., Zhidkov, M. V., Ovanesyan, N. S., Kugabaeva, G. D., & Dzhardimalieva, G. I. (2023). Low-Temperature Synthesis of Metal–Organic Coordination Polymers Based on Oxo-centered Iron Complexes: Magnetic and Adsorption Properties. *Russian Journal of Physical Chemistry A*, *97*(4), 735–748. https://doi.org/10.1134/S0036024423040064

21 Bondarenko, L., Baimuratova, R., Reindl, M., Zach, V., Dzeranov, A., Pankratov, D., Kydralieva, K., Dzhardimalieva, G., Kolb, D., Wagner, F. E., & Schwaminger, S. P. (2024). Dramatic change in the properties of magnetite-modified MOF particles depending on the synthesis approach. *Heliyon*, e27640. https://doi.org/10.1016/j.heliyon.2024.e27640

22 Bennett, T. D., & Cheetham, A. K. (2014). Amorphous Metal–Organic Frameworks. *Accounts of Chemical Research*, *47*(5), 1555–1562. https://doi.org/10.1021/ar5000314

23 Zha, Q., Rui, X., Wei, T., & Xie, Y. (2014). Recent advances in the design strategies for porphyrin-based coordination polymers. *CrystEngComm*, *16*(32), 7371–7384. https://doi.org/10.1039/C4CE00854E

24 Nikoofar, K., & Khademi, Z. (2016). A review on green Lewis acids: Zirconium(IV) oxydichloride octahydrate (ZrOCl2·8H2O) and zirconium(IV) tetrachloride (ZrCl4) in organic chemistry. *Research on Chemical Intermediates*, *42*(5), 3929–3977. https://doi.org/10.1007/s11164-015-2260-6

25 Hou, P., Ma, M., Zhang, P., Cao, J., Liu, H., Xu, X., Yue, H., Tian, G., & Feng, S. (2021). Catalytic transfer hydrogenation of furfural to furfuryl alcohol using easy-to-separate core–shell magnetic zirconium hydroxide. *New Journal of Chemistry*, *45*(5), 2715–2722. https://doi.org/10.1039/D0NJ05638C

26 Cavka, J. H., Jakobsen, S., Olsbye, U., Guillou, N., Lamberti, C., Bordiga, S., & Lillerud, K. P. (2008). A New Zirconium Inorganic Building Brick Forming Metal Organic Frameworks with Exceptional Stability. *Journal of the American Chemical Society*, *130*(42), 13850–13851. https://doi.org/10.1021/ja8057953

27 Deria, P., Chung, Y. G., Snurr, R. Q., Hupp, J. T., & Farha, O. K. (2015). Water stabilization of Zr $_6$ -based metal–organic frameworks via solvent-assisted ligand incorporation. *Chemical Science*, *6*(9), 5172–5176. https://doi.org/10.1039/C5SC01784J

28 Piscopo, C. G., Polyzoidis, A., Schwarzer, M., & Loebbecke, S. (2015). Stability of UiO-66 under acidic treatment: Opportunities and limitations for post-synthetic modifications. *Microporous and Mesoporous Materials*, *208*, 30–35. https://doi.org/10.1016/j.micromeso.2015.01.032

29 Pakamorė, I., Rousseau, J., Rousseau, C., Monflier, E., & Szilágyi, P. Á. (2018). An ambient-temperature aqueous synthesis of zirconium-based metal–organic frameworks. *Green Chemistry*, *20*(23), 5292–5298. https://doi.org/10.1039/C8GC02312C

30 Yang, F., Huang, H., Wang, X., Li, F., Gong, Y., Zhong, C., & Li, J. -R. (2015). Proton Conductivities in Functionalized UiO-66: Tuned Properties, Thermogravimetry Mass, and Molecular Simulation Analyses. *Crystal Growth & Design*, *15*(12), 5827–5833. https://doi.org/10.1021/acs.cgd.5b01190

31 Dutta, S., & Lee, I. S. (2021). Metal–organic framework based catalytic nanoreactors: Synthetic challenges and applications. *Materials Chemistry Frontiers*, *5*(11), 3986–4021. https://doi.org/10.1039/D1QM00242B

32 Rayder, T. M., Bensalah, A. T., Li, B., Byers, J. A., & Tsung, C. -K. (2021). Engineering Second Sphere Interactions in a Host–Guest Multicomponent Catalyst System for the Hydrogenation of Carbon Dioxide to Methanol. *Journal of the American Chemical Society*, *143*(3), 1630–1640. https://doi.org/10.1021/jacs.0c08957

33 Gong, Y., Yuan, Y., Chen, C., Chaemchuen, S., & Verpoort, F. (2020). Palladium metallated shell layer of shell@core MOFs as an example of an efficient catalyst design strategy for effective olefin hydrogenation reaction. *Journal of Catalysis*, *392*, 141–149. https://doi.org/10.1016/j.jcat.2020.09.037

34 Jiang, H., Zhang, W., Kang, X., Cao, Z., Chen, X., Liu, Y., & Cui, Y. (2020). Topology-Based Functionalization of Robust Chiral Zr-Based Metal–Organic Frameworks for Catalytic Enantioselective Hydrogenation. *Journal of the American Chemical Society*, *142*(21), 9642–9652. https://doi.org/10.1021/jacs.0c00637

35 Kassie, A. A., & Wade, C. R. (2020). Catalytic Activity of a Zr MOF Containing POCOP-Pd Pincer Complexes. *Organometallics*, *39*(12), 2214–2221. https://doi.org/10.1021/acs.organomet.0c00164

36 Baimuratova, R. K., Andreeva, A. V., Uflyand, I. E., Shilov, G. V., Bukharbayeva, F. U., Zharmagambetova, A. K., & Dzhardimalieva, G. I. (2022). Synthesis and Catalytic Activity in the Hydrogenation Reaction of Palladium-Doped Metal-Organic Frameworks Based on Oxo-Centered Zirconium Complexes. *Journal of Composites Science*, *6*(10), 299. https://doi.org/10.3390/jcs6100299

37 Zhang, M., Liu, Y., Zhao, H., Tao, J., Geng, N., Li, W., & Zhai, Y. (2021). Pd Anchored on a Phytic Acid/Thiourea Polymer as a Highly Active and Stable Catalyst for the Reduction of Nitroarene. *ACS Applied Materials & Interfaces*, *13*(17), 19904–19914. https://doi.org/10.1021/acsami.0c23007

38 Wang, X., Liang, M., Zhang, J., & Wang, Y. (2007). Selective Hydrogenation of Aromatic Chloronitro Compounds. *Current Organic Chemistry*, *11*(3), 299–314. https://doi.org/10.2174/138527207779940856

39 Jaf, Z. N., Altarawneh, M., Miran, H. A., Almatarneh, M. H., Jiang, Z. -T., & Dlugogorski, Bogdan. Z. (2018). Catalytic Hydrogenation of p -Chloronitrobenzene to p -Chloroaniline Mediated by γ-Mo $_2$ N. *ACS Omega*, *3*(10), 14380–14391. https://doi.org/10.1021/acsomega.8b01936

40 Hennig, C., Weiss, S., Kraus, W., Kretzschmar, J., & Scheinost, A. C. (2017). Solution Species and Crystal Structure of Zr(IV) Acetate. *Inorganic Chemistry*, *56*(5), 2473–2480. https://doi.org/10.1021/acs.inorgchem.6b01624

41 Lowell, S., Shields, J. E., Thomas, M. A., & Thommes, M. (2004). Characterization of Porous Solids and Powders: Surface Area, Pore Size and Density (Vol. 16). Springer Netherlands. https://doi.org/10.1007/978-1-4020-2303-3

42 Tanaka, S. (2020). Mechanochemical synthesis of MOFs. *Metal-Organic Frameworks for Biomedical Applications*, 197–222. Elsevier. https://doi.org/10.1016/B978-0-12-816984-1.00012-3

43 Ghoorchian, A., Afkhami, A., Madrakian, T., & Ahmadi, M. (2020). Electrochemical synthesis of MOFs. *Metal-Organic Frameworks for Biomedical Applications*, 177–195. Elsevier. https://doi.org/10.1016/B978-0-12-816984-1.00011-1

44 Zavyalova, A. G., Kladko, D. V., Chernyshov, I. Yu., & Vinogradov, V. V. (2021). Large MOFs: Synthesis strategies and applications where size matters. *Journal of Materials Chemistry A*, *9*(45), Article 45. https://doi.org/10.1039/D1TA05283G

45 Khan, N. A., & Jhung, S. H. (2015). Synthesis of metal-organic frameworks (MOFs) with microwave or ultrasound: Rapid reaction, phase-selectivity, and size reduction. *Coordination Chemistry Reviews*, *285*, 11–23. https://doi.org/10.1016/j.ccr.2014.10.008

46 Stock, N., & Biswas, S. (2012). Synthesis of Metal-Organic Frameworks (MOFs): Routes to Various MOF Topologies, Morphologies, and Composites. *Chemical Reviews*, *112*(2), 933–969. https://doi.org/10.1021/cr200304e

47 Huang, L. (2003). Synthesis, morphology control, and properties of porous metal–organic coordination polymers. *Microporous and Mesoporous Materials*, *58*(2), 105–114. https://doi.org/10.1016/s1387-1811(02)00609-1

48 Chammingkwan, P., Shangkum, G. Y., Mai, L. T. T., Mohan, P., Thakur, A., Wada, T., & Taniike, T. (2020). Modulator-free approach towards missing-cluster defect formation in Zr-based UiO-66. *RSC Advances*, *10*(47), 28180–28185. https://doi.org/10.1039/D0RA04812G

49 Shearer, G. C., Chavan, S., Bordiga, S., Svelle, S., Olsbye, U., & Lillerud, K. P. (2016). Defect Engineering: Tuning the Porosity and Composition of the Metal–Organic Framework UiO-66 via Modulated Synthesis. *Chemistry of Materials*, *28*(11), 3749–3761. https://doi.org/10.1021/acs.chemmater.6b00602

50 Chen, X., Li, Y., Fu, Q., Qin, H., Lv, J., Yang, K., Zhang, Q., Zhang, H., & Wang, M. (2022). An efficient modulated synthesis of zirconium metal–organic framework UiO-66. *RSC Advances*, *12*(10), 6083–6092. https://doi.org/10.1039/D1RA07848H

51 Feng, Y., Chen, Q., Jiang, M., & Yao, J. (2019). Tailoring the Properties of UiO-66 through Defect Engineering: A Review. *Industrial & Engineering Chemistry Research*, *58*(38), Article 38. https://doi.org/10.1021/acs.iecr.9b03188

52 Feng, X., Jena, H. S., Krishnaraj, C., Leus, K., Wang, G., Chen, H., Jia, C., & Van Der Voort, P. (2021). Generating Catalytic Sites in UiO-66 through Defect Engineering. *ACS Applied Materials & Interfaces*, *13*(51), 60715–60735. https://doi.org/10.1021/acsami.1c13525

53 Feng, D., Wang, K., Wei, Z., Chen, Y. -P., Simon, C. M., Arvapally, R. K., Martin, R. L., Bosch, M., Liu, T. -F., Fordham, S., Yuan, D., Omary, M. A., Haranczyk, M., Smit, B., & Zhou, H. -C. (2014). Kinetically tuned dimensional augmentation as a versatile synthetic route towards robust metal–organic frameworks. *Nature Communications*, *5*(1), 5723. https://doi.org/10.1038/ncomms6723

54 Vetlitsyna-Novikova, K. S., Butova, V. V., Pankin, I. A., Shapovalov, V. V., & Soldatov, A. V. (2019). Zirconium-Based Metal-Organic UiO-66, UiO-66-NDC and MOF-801 Frameworks. Influence of the Linker Effect on the Hydrogen Sorption Efficiency. *Journal of Surface Investigation: X-Ray, Synchrotron and Neutron Techniques*, *13*(5), 787–792. https://doi.org/10.1134/S1027451019050173

55 Zorainy, M. Y., Kaliaguine, S., Gobara, M., Elbasuney, S., & Boffito, D. C. (2022). Microwave-Assisted Synthesis of the Flexible Iron-based MIL-88B Metal–Organic Framework for Advanced Energetic Systems. *Journal of Inorganic and Organometallic Polymers and Materials*, *32*(7), 2538–2556. https://doi.org/10.1007/s10904-022-02353-6

56 Thomas-Hillman, I., Laybourn, A., Dodds, C., & Kingman, S. W. (2018). Realising the environmental benefits of metal–organic frameworks: Recent advances in microwave synthesis. *Journal of Materials Chemistry A*, *6*(25), Article 25. https://doi.org/10.1039/C8TA02919A

57 DeStefano, M. R., Islamoglu, T., Garibay, S. J., Hupp, J. T., & Farha, O. K. (2017). Room-Temperature Synthesis of UiO-66 and Thermal Modulation of Densities of Defect Sites. *Chemistry of Materials*, *29*(3), 1357–1361. https://doi.org/10.1021/acs.chemmater.6b05115

58 Taddei, M., Van Bokhoven, J. A., & Ranocchiari, M. (2020). Influence of Water in the Synthesis of the Zirconium-Based Metal–Organic Framework UiO-66: Isolation and Reactivity of [ZrCl(OH) $_2$ (DMF) $_2$]Cl. *Inorganic Chemistry*, *59*(11), 7860–7868. https://doi.org/10.1021/acs.inorgchem.0c00991